J Mater Sci (2011) 46:101–107
DOI 10.1007/s10853-010-4844-2

Inclusion interaction and effective material properties in a particle-filled composite material system

Siva P. Gurrum · Jie-Hua Zhao · Darvin R. Edwards

Received: 22 January 2010 / Accepted: 16 August 2010 / Published online: 27 August 2010

Abstract This work presents a methodology implementing random packing of spheres combined with commercial finite element method (FEM) software to optimize the material properties, such as Young's modulus, Poisson's ratio, and coefficient of thermal expansion (CTE) of two-phase materials used in electronic packaging. The methodology includes an implementation of a numerical algorithm of random packing of spheres and a technique for creating conformal FEM mesh of a large aggregate of particles embedded in a medium. We explored the random packing of spheres with different diameters using particle generation algorithms coded in MATLAB. The FEM meshes were generated using software MATLAB and TETGEN. After importing the databases of the nodes and elements into commercial FEM software ANSYS, the composite materials with spherical fillers and the polymer matrix were modeled using ANSYS. The effective Young's modulus, Poisson's ratio, and CTE along different axes were calculated using ANSYS by applying proper loading and boundary conditions. It was found that the composite material was virtually isotropic. The Young's modulus and Poisson's ratio calculated by FEM models were compared to a number of analytical solutions in the literature. For low volume fraction of filler content, the FEM results and analytical solutions agree well. However, for high volume fraction of filler content, there is some discrepancy between FEM and analytical models and also among the analytical models themselves. The discrepancy is attributed to the multi-body interaction effect of the filler particles when they are getting close.

S. P. Gurrum · J.-H. Zhao (✉) · D. R. Edwards
Texas Instruments Incorporated, MS3611, 13020 TI Blvd, Dallas, TX 75243, USA
e-mail: jhzhao@ti.com

Introduction

An optimized material set is key to ensuring that a microelectronic package meets performance and reliability requirements. Packaging materials, such as mold compounds, die attach adhesives, underfill materials, and thermal interface materials, are primarily two-phase composite materials. One phase is a polymeric matrix material, such as epoxy or silicone. The other phase is a filler material, such as tiny glass beads, tiny ceramic beads, or metal flakes. The state-of-the-art material manufacturing of these two-phase materials has to ensure that the two phases blend uniformly, adhere well together, and have the desired effective properties. A change in the filler or matrix material, or a change in the filler distribution, affects all the material properties to varying extents.

Several studies have investigated analytical approaches to calculate effective properties of composite materials. Kuster and Toksoz [1] considered the propagation of seismic waves through the composite media to derive effective properties. Devaney and Levine [2] derived effective bulk and shear moduli of random spheres in a matrix using self-consistent formulation of multiple scattering theory. Marur [3] used a three-phase spherical model and rule-of-mixtures to calculate effective properties. Qu and Wong [4] derived expressions for effective elastic modulus using Mori–Tanaka approach. Ju and Chen [5] used an ensemble-micromechanical approach to estimate effective properties.

Analytical approaches are attractive due to their simplicity, but can only yield bulk properties. With decreasing

package form-factors, localized effects due to particle size and distribution may become important. In addition, most of the approaches cannot account for particle size distribution. Computer-aided design tools, such as the finite element method (FEM) software, can play an important role in the optimization of composite materials considering the multitude of physical parameters involved. FEM-based method involves mesh generation, which is difficult for systems with a large number of particle inclusions, especially with close-packed particles. To avoid this issue, different approaches have been reported. Representative volume element (RVE) or unit cell method is widely used. Yang et al. used the RVE method with part of a filler particle with epoxy resin in a cubic RVE to model mold compounds [6]. Bohm and Han have demonstrated that the FEM can be used in a system with 20 particles in a unit cell [7]. The other category of mitigating the difficulty of the FEM mesh generation is to use non-conformal mesh to approximate the interface of filler particles and the matrix resin [8–10]. A non-conformal mesh uses a large number of small brick-shaped elements to divide the space first. Then, the material property is assigned to the small brick elements according to their locations. The mesh generated by this method has "steps" at the phase interfaces. Although there is challenge on conformal mesh generation, nevertheless, it had been demonstrated that the FEM-based models are used for relatively small number (less than 20) [11] or moderate number of particles (about 100 particles) [12] in loosely packed systems with conformal meshes.

To mitigate of the mesh-generation difficulty, one can use totally different modeling paradigm, such as meshless method. In modeling thermal interface material systems of large number of particles (larger than 1,000) with random close-packing of volumetric packing density of about 40–55%, Kanuparthi et al. have demonstrated a meshless method using a home-made numerical code [13, 14].

This work will present a methodology for using random packing of spheres combined with commercial FEM software to optimize the material properties, such as Young's modulus, Poisson's ratio, and coefficient of thermal expansion of two-phase materials used in electronic packaging. A major challenge of the numerical modeling is the proper algorithm of the random packing of spheres and a technique to create conformal finite element mesh of a large aggregate of particles embedded in a medium. This task is non-trivial for handling high packing density of some real materials such as mold compounds and die attach materials (more than 80% weight of filler). We will explore the random packing of spheres with different diameters using particle generation algorithms coded in MATLAB. The composite materials with spherical filler and the polymer matrix will be modeled using a combination of FEM software. This approach can be applied to optimize the materials, as well as to study localized effects near walls.

Particle generation and meshing methodology

It is non-trivial to generate a random particle set of a given radius distribution while still achieving high packing fraction. This article implements the approach outlined by He et al. [15] for generating the radii and coordinates of particles in a box. The particle generation simulation begins by randomly placing the particles of any given radius distribution in a highly constrained box. There is no check for overlap between particles at this stage. The simulation proceeds by relaxing the particles to reduce inter-particle overlap, and by simultaneously increasing the box size to accommodate the increase in volume. Periodic boundary conditions are applied on all the faces of the box to eliminate the effect of impenetrable walls. The simulation ends once the overlap region becomes negligible. This methodology easily achieves volume fractions greater than 0.6 for a periodic box. In the present work, a closed box is simulated to avoid the challenge of sectioning and meshing of spheres intersecting the walls. As a result, the volume fraction is lower due to the wall effect. An artificial lower limit of 1×10^{-3} is imposed for the gap between the wall and particle to avoid floating point errors during mesh generation. This same limit is applied for minimum gaps between the particles. Figure 1 shows the radius distribution for the cases investigated in this study. The solid curve is the theoretical log-normal distribution with the probability density function of particle radius r [15].

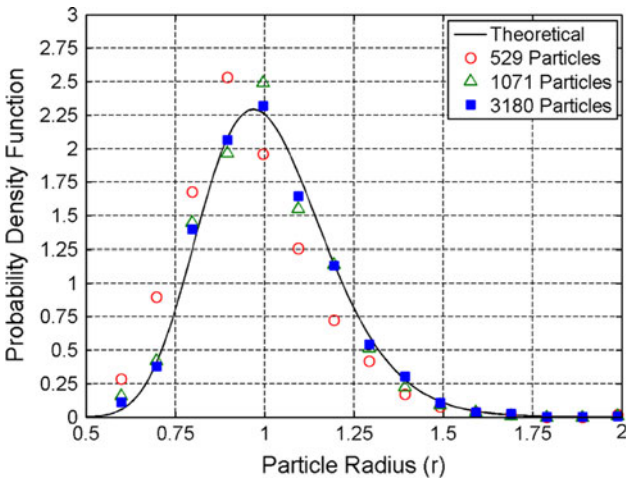

Fig. 1 A comparison of probability density function between theoretical log-normal distribution and simulated cases. The system with 3,180 particles closely follows the target theoretical curve. Higher particle count will reduce this deviation further (Color figure online)

$$f(r) = \frac{1}{\sqrt{2\pi}\sigma r}\exp\left[-(\ln r - \ln r_0)^2 \Big/ (2\sigma^2)\right] \quad (1)$$

where ln r_0 and σ are mean and the standard deviation. In this study, the mean of the particle radii is normalized to be 1, which corresponds to ln $r_0 = 0$, and the standard deviation is chosen to be $\sigma = 0.177$.

From Fig. 1, it is clear that for small size samples (e.g., the 529-particle sample), there is a deviation between the simulated particle size distribution and the target theoretical log-normal distribution. As the number of a particles increases (e.g., the 3,180-particle sample), the simulated distribution follows the target theoretical curve closely.

Generating a conformal finite element mesh over the particle-resin composite system is challenging when the number of particles is large. Most meshing routines become unstable or prohibitively slow during Boolean operations associated with defining the resin volume surrounding the particles. The particle set with radius distribution is meshed using a combination of COMSOL® [16] and TETGEN© [17]. Each spherical particle is first meshed independently in COMSOL® and stored. The collection of all external element faces of all spheres, with additional facets defining the closed box outer walls, is provided as input to TETGEN©. TETGEN efficiently handles tetrahedral meshing of a region bounded by planar facets. The resulting tetrahedral mesh is used for finite element simulations in ANSYS® [18]. This methodology has been applied to a system with 3,180 particles in the present study. Figure 2 shows (a) meshing of a 529-particle composite system with 142,464 nodes and 825,223 elements, (b) meshing of a 1,071-particle composite system with 221,761 nodes and 1,334,197 elements, and (c) meshing of a 3,180-particle composite system with 632,697 nodes and 3,878,693 elements. The mesh is conformal to the particles over the entire region (element faces and nodes match sphere boundaries).

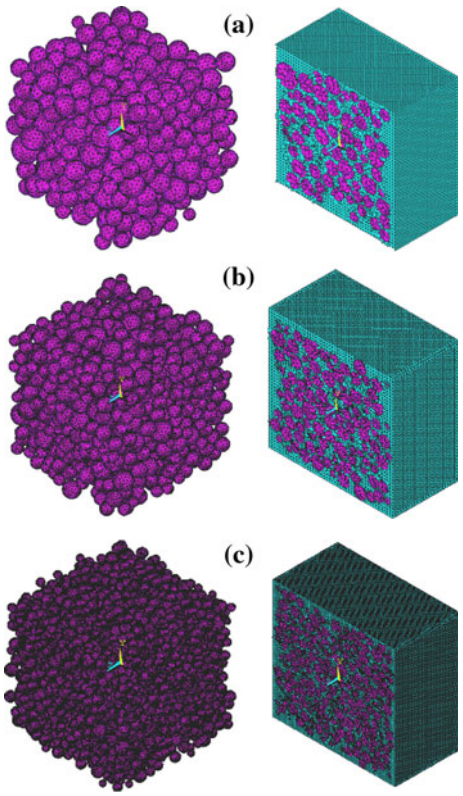

Fig. 2 Meshing of three typical cases: **a** Meshing of a 529-particle composite system with 142,464 nodes and 825,223 elements. **b** Meshing of a 1,071-particle composite system with 221,761 nodes and 1,334,197 elements. **c** Meshing of a 3,180-particle composite system with 632,697 nodes and 3,878,693 elements. The *left images* show independent tetrahedral mesh and the *right images* show the mesh through a section of the simulation domain (Color figure online)

Finite element model for effective properties

The effective material properties of 2-phase composite material, such as Young's modulus, Poisson's ratio, and coefficient of thermal expansion, were studied by virtual experiments (numerical experiments). The FEM calculations were conducted using commercial software ANSYS 10.0 [18]. The ANSYS meshes of filler spheres and matrix resin were generated by importing the nodes definition files and element definition files generated by MATLAB, COMSOL, and TETGEN, which is described in the previous section.

The ANSYS virtual experiments of Young's modulus and Poisson's ratio were conducted by applying tensile loads to the composite material shown in Fig. 3. ANSYS is a general purpose FEM code with implicit integration [18]. Bi-linear 8-node element Solid185 with degenerated tetrahedral option is used for this calculation. In fact, ANSYS provides a few simple commands to change Solid185 element into Solid186 (quadratic 20-node) element by adding mid-side nodes automatically if accurate local stress calculation is needed [18]. To control the total degrees of freedom in a manageable size, Solid185 element is used in this study. For the model with 1,071 particles, the total number of elements is 1,134,197 and the total number of nodes is 221,761. The simulations are performed on a box of the composite material of size L_x, L_y, and L_z along x, y, and z directions, respectively. The box dimension, L_x, L_y, and L_z are around 22 length units for the 1,071-particle model. The exact length may be slightly different due to the random nature of the model. The virtual experiment of tensile modulus (Young's modulus) in x-axis was done by applying 100 MPa tensile stress at the end side of the box ($x = L_x$). The boundary conditions for these experiments are: symmetry boundary conditions at the three faces of

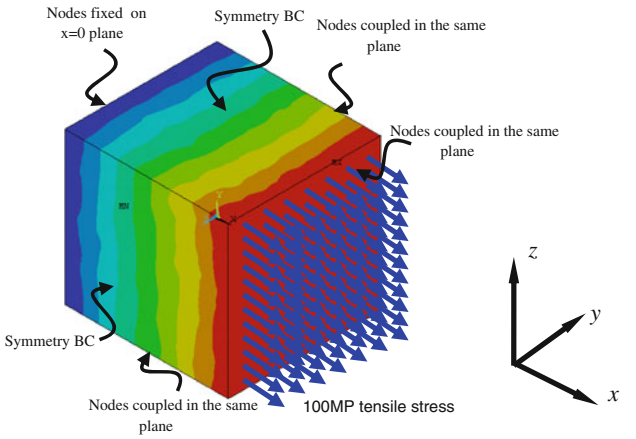

Fig. 3 Loading and boundary conditions for the calculation of effective Young's modulus of the composite along x-direction (E_x). The *color* represents the displacement contour along the x-axis (u_x) (Color figure online)

$x = 0$, $y = 0$, and $z = 0$, coupled-node boundary condition (keeping the nodes in the same plane) at faces $x = L_x$, $y = L_y$, and $z = L_z$. The ANSYS implementation of the coupled-node boundary conditions is that the displacement (e.g., u_x) of the nodes in the selected node set is the same value (e.g., u_x changes with the external load, however, u_x of all nodes in the node set equals each other) [18]. The coupled-node boundary condition is applied since particles and the resin have different moduli and Poisson's ratios. As a result, the boundary will not be smooth when the composite block is under tensile load. The un-even surfaces make the deformation measurement hard to define. The coupled-node boundary condition eliminates this difficulty. It also represents the condition that the composite block is an inclusion in an infinitely large composite consisting of the same filler particles and matrix. The response of the tensile test is characterized by extension of the composite block in x-axis (u_x) and the contractions in both y-axis (u_y) and z-axis (u_z). The strains along x-, y-, and z-axes are, therefore [19]:

$$\varepsilon_x = \frac{u_x}{L_x}, \tag{2}$$

$$\varepsilon_y = \frac{u_y}{L_y}, \tag{3}$$

$$\varepsilon_z = \frac{u_z}{L_z}. \tag{4}$$

Young's modulus along the x-axis is then

$$E_x = \frac{\sigma_x}{\varepsilon_x}. \tag{5}$$

Poison's ratios are:

$$v_{xy} = -\frac{\varepsilon_y}{\varepsilon_x}, \tag{6}$$

and

$$v_{xz} = -\frac{\varepsilon_z}{\varepsilon_x}. \tag{7}$$

The same procedure was applied to evaluate the Young's modulus along y-axis (E_y) and z-axis (E_z) and the Poisson's ratios v_{yx}, v_{yz}, v_{zx}, and v_{zy} [19].

In the virtual experiments used to obtain the coefficient of thermal expansion, the boundary conditions are the same as the ones used for the Young's modulus experiments, except for the loading condition. Instead of applying tensile stress as the load, a uniform temperature drop of 1 °C was applied on all nodes, see Fig. 4 for detail. This results in thermal contraction along the x-, y-, and z-axes. By definition, the CTEs in x-, y-, and z-axes were obtained by computing the contraction thermal strains along the corresponding directions. The color contour represents the displacement contour along the x-axis (u_x).

Results and discussion

In this study, the filler particles were tiny glass beads with Young's modulus of 72.9 GPa, Poisson's ratio of 0.17, and CTE of 0.5 ppm/°C. The resin matrix was epoxy with Young's modulus of 5.55 GPa, Poisson's ratio of 0.33, and CTE of 55 ppm/°C. The results are tabulated in Table 1 and Table 2 for different filler volume fractions.

Comparing the tensile moduli, Poisson's ratios, and CTEs along different directions, it is clear that these values are not sensitive to direction. It is reasonable to assume that the composite material behaves as an isotropic material macroscopically. The Young's modulus, Poisson's ratio, and CTE were obtained for the isotropic material by averaging the corresponding properties over different directions. The properties of the isotropic material are listed in Table 3.

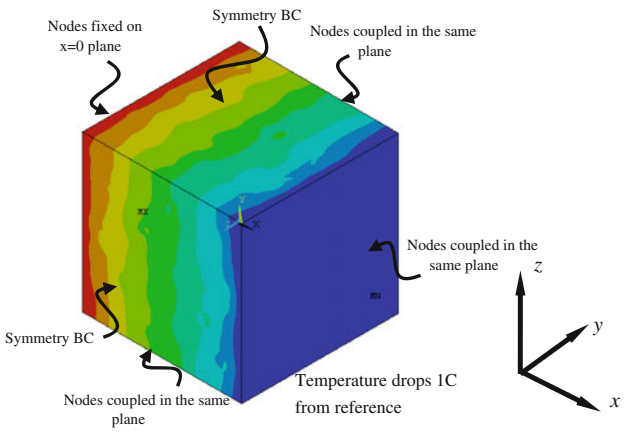

Fig. 4 Loading and boundary conditions for the calculation of effective CTE of the composite along x-direction (CTE_x). Temperature load is 1 °C drop at all nodes from the reference temperature. The *color* represents the displacement contour along the x-axis (u_x) (Color figure online)

Table 1 Young's moduli and Poisson's ratios along three orthogonal axes calculated by FEM virtual experiments for different filler volume fractions

Filler volume fraction	E_x (MPa)	E_y (MPa)	E_z (MPa)	v_{xy}	v_{xz}	v_{yx}	v_{yz}	v_{zy}	v_{zx}
0.233	9731.9	9720.1	9731.2	0.2846	0.2834	0.2842	0.2844	0.2847	0.2834
0.303	11816	11792	11820	0.2661	0.2639	0.2656	0.2655	0.2662	0.2640
0.403	15682	15660	15707	0.2414	0.2387	0.2411	0.2402	0.2409	0.2391
0.432	17061	17105	17099	0.2329	0.2309	0.2335	0.2319	0.2318	0.2314
0.476	18874	18954	18976	0.2267	0.2246	0.2276	0.2248	0.2251	0.2258

Table 2 CTE along three orthogonal axes calculated by FEM virtual experiments for different filler volume fractions

Filler volume fraction	CTE_x (ppm/°C)	CTE_y (ppm/°C)	CTE_z (ppm/°C)
0.233	37.4	37.4	37.2
0.303	32.6	32.6	32.4
0.403	25.7	25.6	25.5
0.432	23.9	23.7	23.9
0.476	21.4	21.2	21.6

Table 3 CTE, Young's modulus, and Poisson's ratio of the composite as a function of filler volume fraction

Filler volume fraction	CTE_{eff} (ppm/°C)	E_{eff} (GPa)	v_{eff}
0	55.0	5.550	0.3300
0.233	37.3	9.728	0.2841
0.303	32.5	11.809	0.2652
0.403	25.6	15.683	0.2402
0.432	23.8	17.088	0.2321
0.476	21.4	18.935	0.2258

The values are the average of the values around three orthogonal directions by taking the advantage of the near isotropic nature of the composite system

The effective Young's modulus and effective Poisson's ratio have been studied by several investigators. However, almost every method uses approximations. For example, Devaney and Levine [2] used a self-consistent formulation of multiple scattering theory to deduce the relationship of bulk modulus (K) and shear modulus (G) of the constituents and the effective properties of the composite:

$$K_{\text{eff}} = K_{\text{m}} + c\frac{(3K_{\text{eff}} + 4G_{\text{eff}})(K_{\text{i}} - K_{\text{m}})}{3K_{\text{eff}} + 4G_{\text{eff}} + 3(K_{\text{i}} - K_{\text{m}})} \tag{8}$$

$$G_{\text{eff}} = G_{\text{m}} + c\frac{5(3K_{\text{eff}} + 4G_{\text{eff}})G_{\text{eff}}(G_{\text{i}} - G_{\text{m}})}{(15K_{\text{eff}} + 20G_{\text{eff}})G_{\text{eff}} + 6(K_{\text{eff}} + 2G_{\text{eff}})(G_{\text{i}} - G_{\text{m}})} \tag{9}$$

where the subscript "i" indicates the inclusion (filler in our case), "m" indicates the matrix (epoxy resin in our case), "c" is volume fraction of inclusion (filler), and "eff" indicates the effective properties of the composite material. These equations need to be solved numerically for the effective bulk modulus and shear modulus. General mathematics software package Mathematica [20] was used to solve the coupled Eqs. 8 and 9.

Young's modulus (E) and Poisson's ratio (v) are related to bulk modulus (K) and shear modulus (G) by the following relations for isotropic materials [21]:

$$G = \frac{E}{2(1+v)} \tag{10}$$

$$K = \frac{E}{3(1-2v)} \tag{11}$$

or equivalently,

$$E = 3(1-2v)K \tag{12}$$

$$v = \frac{3K - 2G}{2(3K+G)} \tag{13}$$

Kuster and Toksoz [1] used seismic wave scattering method to treat the two-phase material with inclusions in the matrix and get the effective bulk modulus and effective shear modulus:

$$K_{\text{eff}} = K_{\text{m}} + c\frac{(3K_{\text{eff}} + 4G_{\text{eff}})(K_{\text{i}} - K_{\text{m}})}{3K_{\text{i}} + 4G_{\text{eff}}}, \tag{14}$$

$$G_{\text{eff}} = G_{\text{m}} + c\frac{6G_{\text{eff}}(K_{\text{m}} + 2G_{\text{m}})(G_{\text{i}} - G_{\text{m}}) + G_{\text{m}}(9K_{\text{m}} + 8G_{\text{m}})(G_{\text{i}} - G_{\text{m}})}{6G_{\text{i}}(K_{\text{m}} + 2G_{\text{m}}) + G_{\text{m}}(9K_{\text{m}} + 8G_{\text{m}})}. \tag{15}$$

Qu and Wong [4] presented a Mori–Tanaka model for the effective property of underfill materials:

$$K_{\text{eff}} = K_{\text{m}}\left\{1 + \frac{c(K_{\text{i}} - K_{\text{m}})}{K_{\text{m}} + 3\gamma_{\text{m}}(1-c)(K_{\text{i}} - K_{\text{m}})}\right\}, \tag{16}$$

$$G_{\text{eff}} = G_{\text{m}}\left\{1 + \frac{c(G_{\text{i}} - G_{\text{m}})}{G_{\text{m}} + 2\delta_{\text{m}}(1-c)(K_{\text{i}} - K_{\text{m}})}\right\}, \tag{17}$$

where

$$\gamma_{\text{m}} = \frac{1 + v_{\text{m}}}{9(1 - v_{\text{m}})}, \tag{18}$$

$$\delta_m = \frac{4 - 5\nu_m}{15(1 - \nu_m)}. \quad (19)$$

Marur [3] used a three-phase spherical model to deduce the effective bulk modulus of the particulate composite:

$$K_{eff} = K_m \frac{\beta(1 + \gamma c) + \gamma(1 - c)}{\beta(1 - c) + (\gamma + c)} \quad (20)$$

where $\beta = K_i/K_m$ and $\gamma = (4G_m)/(3K_m)$.

Marur also assumed that the rule-of-mixture applies to Poisson's ratio:

$$\nu_{eff} = c\nu_i + (1 - c)\nu_m. \quad (21)$$

Ju and Chen [5] provided an approximate model considering the interactions between particles. The effective bulk modulus and shear modulus are:

$$K_{eff} = K_m \left\{ 1 + \frac{30(1 - \nu_m)c(3\gamma_1 + 2\gamma_2)}{3\alpha + 2\beta - 10(1 + \nu_m)c(3\gamma_1 + 2\gamma_2)} \right\}, \quad (22)$$

$$G_{eff} = G_m \left\{ 1 + \frac{30(1 - \nu_m)c\gamma_2}{\beta - 4(4 - 5\nu_m)c\gamma_2} \right\}, \quad (23)$$

where

$$\alpha = 2(5\nu_m - 1) + 10(1 - \nu_m)\left(\frac{K_m}{K_i - K_m} - \frac{G_m}{G_i - G_m} \right), \quad (24)$$

$$\beta = 2(4 - 5\nu_m) + 15(1 - \nu_m)\frac{G_m}{G_1 - G_m}, \quad (25)$$

$$\gamma_1 = \frac{5c}{96\beta^2}\left\{ 12\nu_m(13 - 14\nu_m) - \frac{96\alpha}{3\alpha + 2\beta}(1 - 2\nu_m)(1 + \nu_m) \right\}, \quad (26)$$

$$\gamma_2 = \frac{1}{2} + \frac{5c}{96\beta^2} \times \left\{ 6(25 - 34\nu_m + 22\nu_m^2) - \frac{36\alpha}{3\alpha + 2\beta}(1 - 2\nu_m)(1 + \nu_m) \right\}. \quad (27)$$

Since some of the analytical solutions are for particles with a single diameter and the maximum volume fraction of single size particles is about 0.64 for random packing, the comparison of the analytical results and the FEM results are plotted against each other for filler volume fraction from 0 to 0.65 in Figs. 5 and 6. The calculated Young's modulus and Poisson's ratio by FEM are fitted by second order polynomials.

In Fig. 5, in region of low volume fraction of filler, the FEM results and analytical solutions agree well. However, for high volume fraction of filler, the FEM calculated results are consistently higher than all the analytical results. This is due to several reasons. Firstly, it is due to the multi-body interactions of filler particles when they are getting closer. The FEM calculation can take this multi-body interaction into account fully, however, the analytical solutions can only partially account for the interaction due to various approximations. Secondly, the spheres in FEM simulations have a diameter distribution, but some analytical solutions are for particles of a single diameter. Thirdly, there could be some artifact of the sidewall effect of the FEM meshes. In our FEM meshes, the filler spheres are all located inside the six boundaries of the box. There is no sphere cutting through any boundary. If the box dimensions are infinitely large and the particle number is also infinitely large, the effect of walls would be negligible. However, due to the limited dimensions of the box simulated in this work, the wall effect is probably not negligible. The volume fraction drops near the walls due to the shape of the particles, whereas the inner region has a much higher volume fraction.

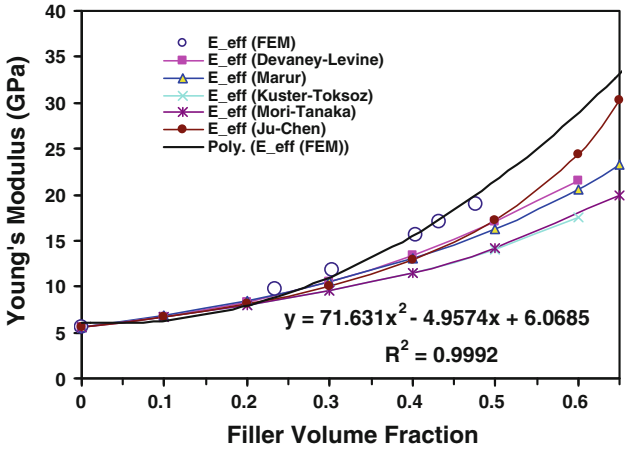

Fig. 5 Young's modulus as a function of filler volume fraction. A comparison of FEM-calculated results and different analytical solutions are plotted against each other

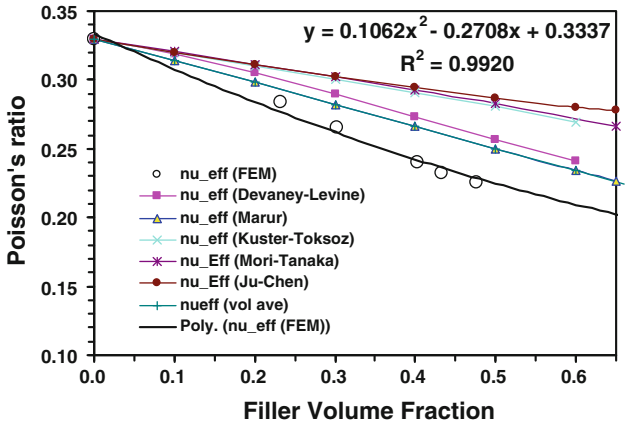

Fig. 6 Poisson's ratio as a function of filler volume fraction. A comparison of FEM-calculated results and different analytical solutions are plotted against each other

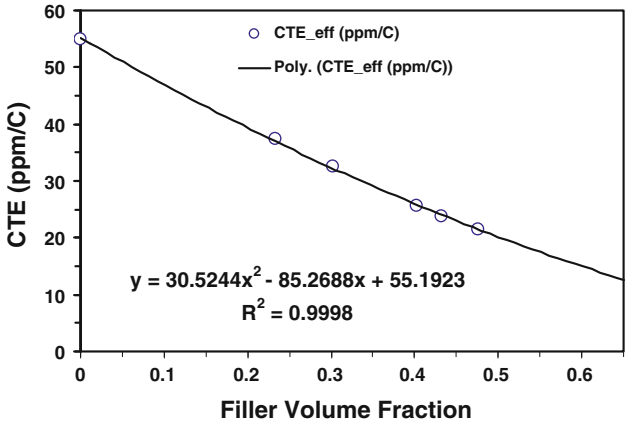

Fig. 7 Effective CTE calculated by the FEM as a function of filler volume fraction

The CTE values of the composite material are plotted against the volume fraction of the filler in Fig. 7. The CTE decreases as the filler content increases. A second order polynomial fit is also shown for the CTE of the composite. The fact that Young's modulus and CTE have a second order relationship to the filler content is a good indication of the strong interaction of filler particles. Otherwise, simple relationships such as the "rule-of-mixtures" will give linear relation between the modulus and filler content, and "modulus-modified rule-of-mixtures" will also give linear relation between CTE and filler content [22].

Conclusions

This article describes an FEM-based methodology to calculate effective properties of composite materials. The methodology can simulate an arbitrary particle distribution with a fully conforming mesh of the particle-resin matrix. The Young's modulus predicted by the FEM-based methodology is higher than existing analytical solutions at large volume fractions (higher than 0.4). This is likely due to the multi-body interactions of filler particles when they are getting closer. The FEM calculation can take this multi-body interaction into full account, however, the analytical solutions can only partially account for the interaction due to various approximations. Further work is in progress to develop a model with particles intersecting the boundaries of the simulated domain, so as to simulate a homogenous material. The methodology presented here can be used to optimize particle-filled composite materials, as well as to study localized effects near the walls of such composite materials.

References

1. Kuster GT, Toksoz MN (1974) Geophysics 39:587
2. Devaney J, Levine H (1980) Appl Phys Lett 37:377
3. Marur PR (2004) Mater Lett 58:3971
4. Qu J, Wong CP (2002) IEEE Trans Compon Packag Technol 25:53
5. Ju JW, Chen TM (1994) Acta Mech 103:123
6. Yang D, Jansen KMB, Wang LG, Ernst LJ, Zhang GQ, Bressers HJL, Fan X (2004) IEEE Trans Compon Packag Technol 27:676
7. Bohm HJ, Han W (2001) Model Simul Mater Sci Eng 9:47
8. Guessasma S, Babin P, Della Valle G, Dendievel R (2008) Int J Solids Struct 45:2881
9. Guessasma S, Bassir D (2010) Acta Mater 58:716
10. Xu Y, Yagi K (2004) Comput Mater Sci 30:242
11. Chawla N, Sidhu RS, Ganesh VV (2006) Acta Mater 54:1541
12. Chawla N, Ganesh VV, Wunsch B (2004) Scripta Mater 51:161
13. Kanuparthi S, Subbarayan G, Siegmund T, Sammakia B (2009) IEEE Trans Compon Packag Technol 32:424
14. Kanuparthi S, Subbarayan G, Siegmund T, Sammakia B (2008) IEEE Trans Compon Packag Technol 31:611
15. He D, Ekere NN, Cai L (1999) Phys Rev E 60:7098
16. Comsol Multiphysics 3.3, User's Manual, Comsol Inc., http://www.comsol.com/
17. Si H TetGen, available online: http://tetgen.berlios.de/
18. ANSYS 10.0 User's Manual, Ansys Inc., available online, http://www.ansys.com/
19. Kollar LP, Springer GS (2003) Mechanics of composite structures, chap 2. Cambridge University Press, Cambridge
20. Mathematica 6 Documentation, available online: http://www.wolfram.com/
21. Chou PC, Pagano NJ (1992) Elasticity. Dover Publications, Mineola, NY
22. Wu TY, Guo Y, Chen WT (1993) IBM J Res Dev 37:621